Design of Force Sensing Smart Robot Finger using Embedded Fiber Bragg Grating Sensors via Shape Deposition Manufacturing

Yong-Lae Park[1], Kelvin Chau[2], Richard J. Black[2], and Mark R. Cutkosky[1]

[1]Center for Design Research, Stanford University
Stanford, CA 94305-2232, USA
contact: ylpark@stanford.edu

[2]Intelligent Fiber Optic Systems
2363 Calle Del Mundo, Santa Clara, CA 95054, USA

***Abstract*— Force sensing is an essential requirement for dexterous robot manipulation. Although strain gages have been widely used, a new sensing approach is desirable for applications that require greater robustness, design flexibility and immunity to electromagnetic noise. An exoskeletal force sensing robot finger was developed by embedding Fiber Bragg Grating (FBG) sensors into a polymer-based structure. Multiple FBG sensors were embedded into the structure to allow the manipulator to sense and measure both contact forces and grasping forces. In order to fabricate a three-dimensional structure, a new shape deposition manufacturing (SDM) process was explored. The sensorized SDM-fabricated finger was then characterized using an FBG interrogator. A force localization scheme is also described.**

I. Introduction

Future robots are expected to free human operators from difficult and dangerous tasks requiring high dexterity in various environments. One example is extra-vehicular repair of a manned spacecraft that would otherwise require hazardous work by human astronauts. Operating complicated tools and performing repairs requires a manipulator of great precision and coordination. Therefore, force sensing is one of the most critical requirements for this type of robot control.

However, compared to even the simplest of animals, today's robots are impoverished in terms of their sensing abilities. For example, a single spider can contain as much as 325 mechanoreceptors on its legs [2], in addition to hair sensors, chemical sensors, etc.[1], [16]. Mechanoreceptors such as the slit sensilla of spiders [2], [5] and campaniform sensilla of insects [12], [17] are especially concentrated near the joints, where they provide the animals with extensive information about loads imposed on the limbs – whether due to normal activities such as running or grasping prey, or as the result of unexpected events such as collisions. In contrast, robots generally have a modest number of mechanical sensors, often associated with actuators or concentrated in a special device such as a force sensing wrist. As a result, robots often poorly identify and respond to unexpected and arbitrarily-located impacts.

The work in this paper is part of a broader effort aimed at creating light-weight, rugged appendages for robots that, like the exoskeleton of an insect, feature embedded sensors so that the robot can be more aware of both anticipated and unanticipated loads. We focus on a particular class of optical sensors, Fiber Bragg Grating (FBG) sensors, that have been identified as promising for space robotics and other applications where high sensitivity, multiplexing capability, and immunity to electromagnetic noise and electrical passivity are particularly desirable. The sensors consist of optical fibers with Bragg cell gratings that measure local strains, which are proportional to the shift in the peak wavelength (Bragg wavelength) reflected by the FBG. Typical values for the sensitivity to an axial strain are 1 nm/millistrain at 1300 nm and 0.64 nm/millistrain at 820 nm center wavelengths [9]. This sensitivity consistently yields better resolution and accuracy than 0.8 microstrain and 4 microstrain, respectively. In addition, the strain response is linear with no indication of hysteresis at temperatures as high as 370°C [13]. Multiple FBG sensors can be placed along a single fiber and optically multiplexed. Such multiplexing capability is another very attractive feature of FBG sensors in comparison with, for example, traditional resistive foil strain gages.

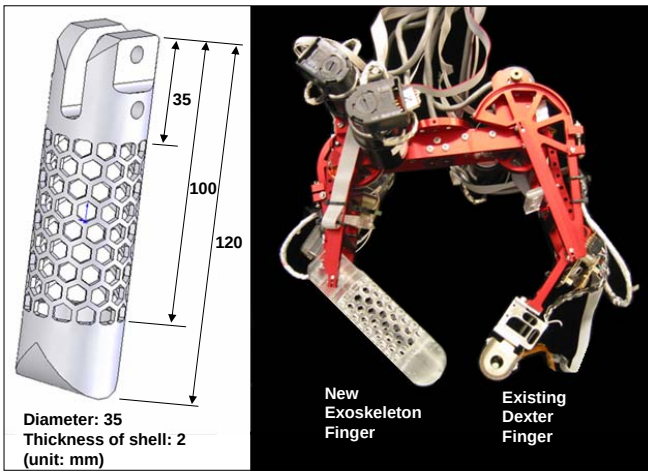

Fig. 1. Prototype dimensions and Dexter manipulator

FBG sensors have previously been embedded in metal parts [10] and composites [19] to monitor stresses. To our knowledge this is their first application in hollow, multi-material structures made by a rapid-prototyping process. In

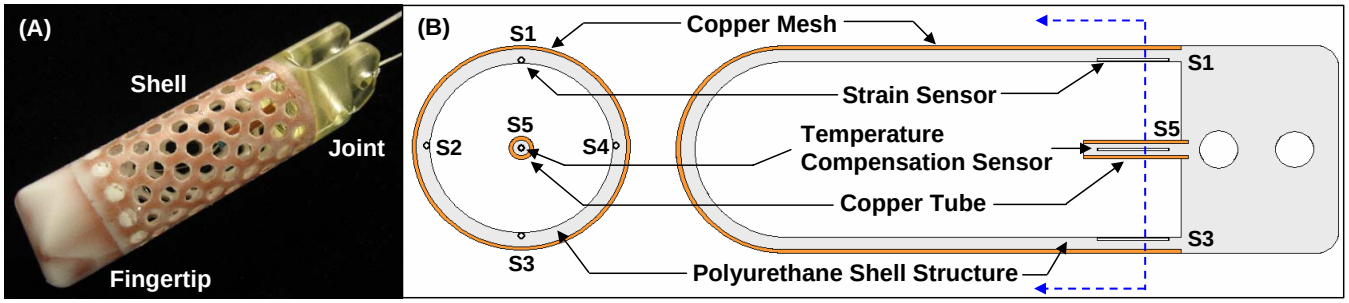

Fig. 2. (A) Complete finger prototype (B) Cross-sectional views (s1-s4: strain sensors, s5: temperature compensation sensor)

this paper we describe the rapid prototyping process and its adaptation to allow the embedding of optical fiber sensors. The results of a first prototype revealed the need to embed a thermal shield to reduce the effects of external temperature variations. Accordingly, a second prototype was developed with an embedded copper mesh in addition to four fiber optic sensors. The results of tests performed on this prototype are reported and the implications for use in force control as well as collision detection are discussed. We conclude with a discussion of future work, including extensions to larger numbers of sensors so that a more complete picture of external force magnitudes and contact locations can be obtained.

II. Design Concept

Figure 2 shows the completed finger prototype and its cross-sectional views. The finger can be divided into three parts: fingertip, shell, and joint. The fingertip and shell are hollow, exoskeletal structures. Four FBG sensors were embedded into the shell for strain measurement, and one FBG sensor was placed in the middle of the structure for temperature compensation. Since the prototype will replace the lower finger of the Dexter [7] manipulator as shown in Figure 1, its dimensions have been set accordingly.

A. Exoskeletal Structure

The exoskeletal structure is light weight while maintaining relatively high strength. Since the structure deforms not only locally but globally depending on the location of force application, the finger is able to measure and localize applied forces intrinsically as well as extrinsically. This is useful for both grasp force measurement and collision detection.

A plastic shell fingertip has been proposed by Voyles et al. [20] for extrinsic tactile sensing using electrorheological fluids. However, it was necessary to make an additional cantilever beam structure to install strain gages to obtain force-torque information for intrinsic tactile sensing [4]. The prototype discussed in this paper requires only a shell structure to provide force information for both extrinsic and intrinsic sensing.

B. Hexagonal Shell Pattern

The prototype has a hexagonally patterned shell. This pattern allows the structure to concentrate stresses and strains on the narrow ribs, facilitates embedded sensor placement and has an added effect of amplifying the sensor signal.

Although two other regular polygons, triangles and squares, can also be used exclusively to form the shell pattern, the hexagon minimizes the ratio of perimeter to area [14], which has been mathematically proven by Hales [8]. In addition, the hexagonal cells avoid sharp interior corners which could reduce the fatigue life. In summary, the hexagonal structure can minimize the amount of material for fabrication and the weight of the part while providing high structural strength.

C. Creep Prevention and Thermal Shielding

Polymer structures unavoidably experience greater creep than metal structures. Creep adversely affects the linearity and repeatability of the embedded sensor output, both of which are mainly dependent on the stiffness and resilience of the structure. In addition, thermal changes can affect the FBG strain sensor outputs. Drawing inspiration from [6], a copper mesh (080X080C0055W36T, TWP Inc., Berkeley, California, USA) was embedded into the outside of the shell, to reduce creep and provide thermal shielding. The high conductivity of copper expedites distribution of heat applied from outside the shell and creates a more uniform temperature gradient inside the shell.

D. Strain Sensor Configuration

More sensors provide more information and make the system more reliable. However, since more sensors require more time and/or processing capacity to handle the larger amount or data, the optimal sensor design should be considered as discussed by Bicchi [3]. Ultimately, the force information we would like to obtain from our system includes longitudinal location, latitudinal location, magnitude of applied force, and orientation of the force vector. For the present, we assume forces are applied only in a normal direction to the surface to simplify the system. Since this assumption reduces the number of unknowns to three, a minimum of three, linearly independent sensors are needed. In the prototype, four strain sensors were embedded in the shell.

Before starting fabrication, finite element analysis was conducted to determine the sensor locations. Figure 3 shows strain distributions when different types of forces are applied to the shell and to the fingertip. Strain is most concentrated

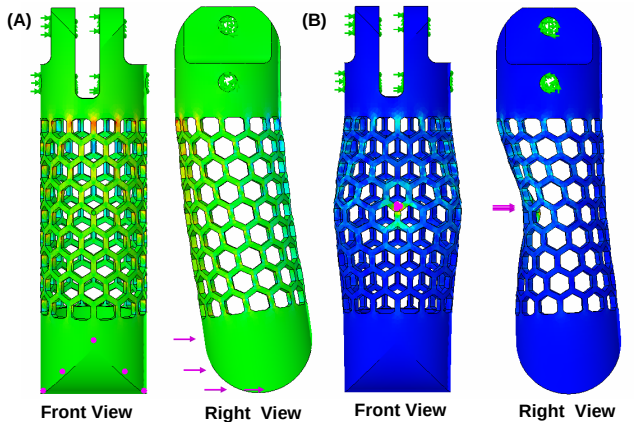

Fig. 3. Finite element analysis of finger prototype

at the top of the shell where it is connected to the joint. Therefore, four sensors were embedded at 90° intervals into the first rib of the shell, closest to the joint, as shown in Figure 2.

E. Temperature Compensation

Since embedded FBG sensors are sensitive to temperature change as well as strain change, it is necessary to isolate thermal effects from mechanical strains. Various complicated temperature compensation methods have been proposed, such as use of dual-wavelength superimposed FBG sensors [22], saturated chirped FBG sensors [23], and a FBG sensor rosette [11]. In contrast, a simpler method is to use an isolated, strain-free FBG sensor to directly measure the thermal effects. Subtracting the wavelength shift of this temperature compensation sensor from that of any other sensor corrects for the thermal effects on the latter [15]. An important assumption in this method is that all sensors are at the same temperature. Our prototype has one temperature compensation sensor in the hollow area in the middle of the shell as shown in Figure 2. Although the temperature compensation sensor is physically removed from the strain sensors, the copper heat shield is expected to create a more uniform temperature gradient inside the shell. The temperature compensation sensor was encapsulated in a stiff copper tube attached at only one end to the joint, and therefore is expected to experience no mechanical strain, regardless of external forces applied to the finger.

III. SDM Fabrication Procedure

Figure 4 shows the steps of the Shape Deposition Manufacturing (SDM) process [21] for the finger prototype fabrication. It is difficult to make hollow three-dimensional parts using conventional SDM processes, since only the top of the part is accessible for machining. Therefore, a modified SDM process was developed and applied for the fabrication of the finger. The prototype was cast in steps with no direct machining. The first step is molding of the shell. The outer mold is made of hard wax to maintain the overall shape. In contrast, the inner mold is hollow and made of soft silicone

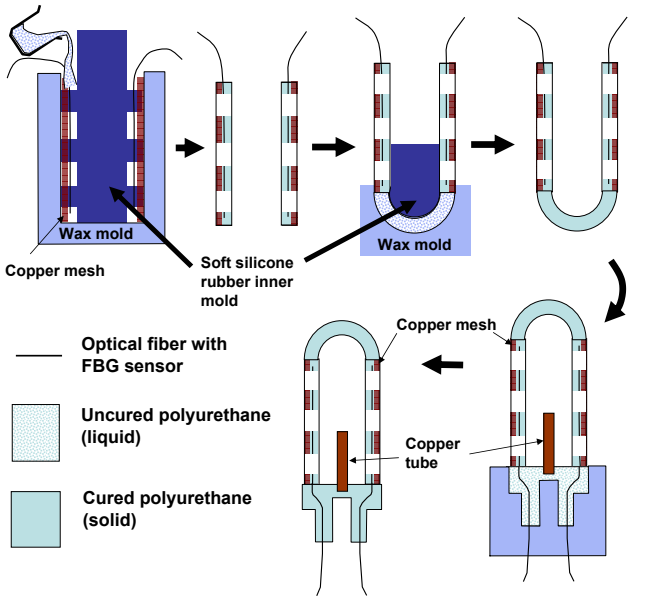

Fig. 4. SDM prototype fabrication process

rubber, which can manually deformed and removed when the polyurethane is cured. The strain sensors and copper mesh are embedded in this step. The second step is fingertip casting, which uses a separate mold and occurs after the shell is fully cured. As it cures, the polyurethane for the fingertip bonds to the cured polyurethane of the shell. In the final step, the joint is cast. As with the fingertip, the joint bonds to the cured shell. Since the joint is not hollow, an inner mold is not needed during this step. Since the joint has no copper mesh, it was cast using a hard, stiff polyurethane (Task 9, Smooth-On, Easton, Pennsylvania, USA) to reduce creep, while the shell and fingertip were both cast from a softer polyurethane (Task 3, Smooth-On, Easton, Pennsylvania, USA).

IV. Force Sensing Test and Evaluation

Three different sets of tests were carried out to evaluate the static, dynamic, and thermal performance of the prototype. The static tests show how linear and repeatable the system is, the dynamic tests how responsive the system is, and the thermal tests how well the system compensates for errors caused by temperature change.

A. Static Tests

Static forces were applied to two different locations on the finger: shell and fingertip. Figure 5 and 6 show the force locations and the responses of two of the four sensors. Applying a force to the shell yielded sensitivities of 0.024nm/N and -0.0044nm/N for sensor A and B, respectively. The optical system can resolve wavelength changes of 0.5pm or less, corresponding to to 0.015N or less for the minimum detectable force change. Note that the A sensor, being on the same side of the shell as the contact force, has a much higher sensitivity to it. Applying a force to the fingertip yielded sensitivities of 0.032 nm/N and -0.029 nm/N. In

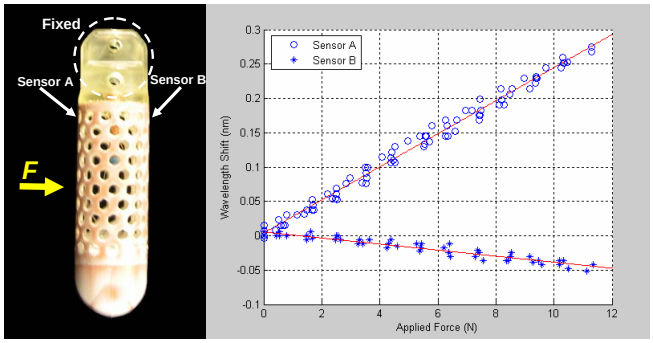

Fig. 5. Shell contact force response test

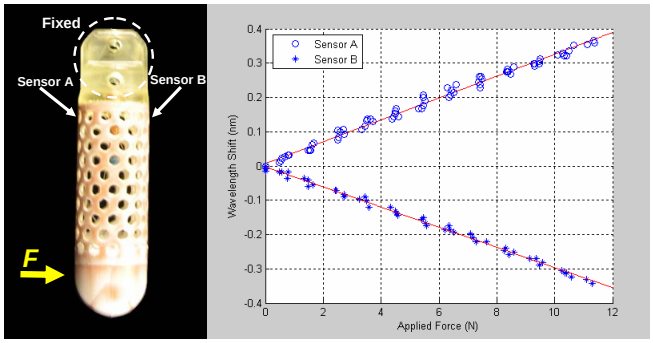

Fig. 6. Fingertip force response test

this case, the location of the force results in roughly equal strains at both sensors. For a given location, the ratio of the two sensor outputs is independent of the magnitude of the applied force. The effect of location is discussed in Section V (Contact Force Localization). The system shows a maximum of 5.3% and 3.9% deviation from a linear response for shell and fingertip tests, respectively.

B. Dynamic Tests

Dynamic force tests were conducted by subjecting the system to a step input, which was generated by quickly removing a weight of 200g (1.962N). The sensor was sampled at 10 kHz, and the output is shown in figure 7. Rise time and settling times were approximately 0.02 seconds and 0.05 seconds, respectively, and less than 2.5% overshoot was observed. Since the signal to noise ratio is 25.25, this system can measure dynamic forces as small as 0.01N at rates greater than 10 Hz.

C. Thermal Effect Tests

Figure 8 shows a typical thermal test result. Over a three minute period, the fingertip was loaded and unloaded at several locations while the temperature was decreased from 28.3°C to 25.7°C. The ideal (temperature invariant) sensor output is indicated by the dashed line. Experiment results show that use of the temperature compensation sensor reduces thermal effects somewhat. However a more accurate compensation design is desired in the next prototype.

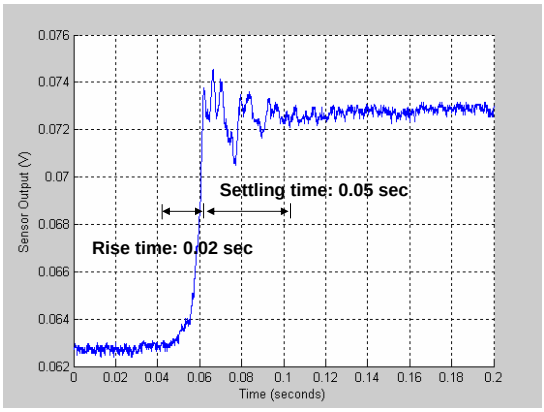

Fig. 7. Step response of strain sensor

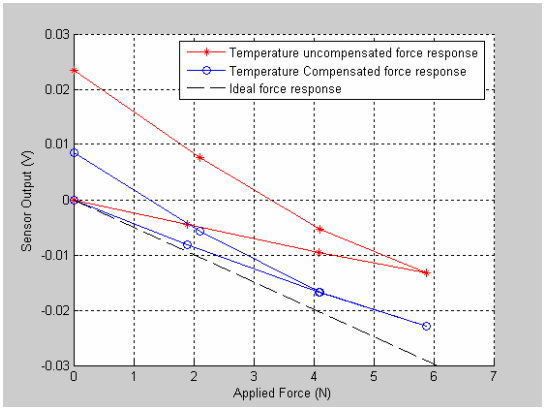

Fig. 8. Varying temperature test result showing partial temperature compensation provided by the central sensor

V. Contact Force Localization

A. Longitudinal Location

Longitudinal localization requires some understanding of structural deformation of the shell. Figure 9 shows simplified two-dimensional diagrams of the prototype. When a force is exerted at a certain location, as shown in (A), the structure will deform and sensors A and B will measure strains ε_A and ε_B, respectively, as indicated in (D). This situation can be decomposed into two separate effects, as shown in (B) and (C). By superposition, $\varepsilon_A = \varepsilon_1 + \varepsilon_2$ and $\varepsilon_B = \varepsilon_3$. Therefore, if the ratio of ε_A to ε_B is known, we can estimate d, the longitudinal location of the applied force. Figure 10 shows the plot of experimental ratios of ε_A to ε_B as a function of d.

There is some ambiguity in the localization, since two values of d result in the same ratio. However, if we let d_0 be the distance at which $\varepsilon_A/\varepsilon_B$ is minimized, and we restrict ourselves the region $d > d_0$, we can resolve the ambiguity. Further, if we modify the manufacturing process to place the sensors closer to the other surface of the shell, d_0 approaches 0 and we can localize an applied force closer to the joint.

B. Latitudinal Location

Latitudinal location can be approximated using centroid and peak detection as discussed by Son et al [18]. Only

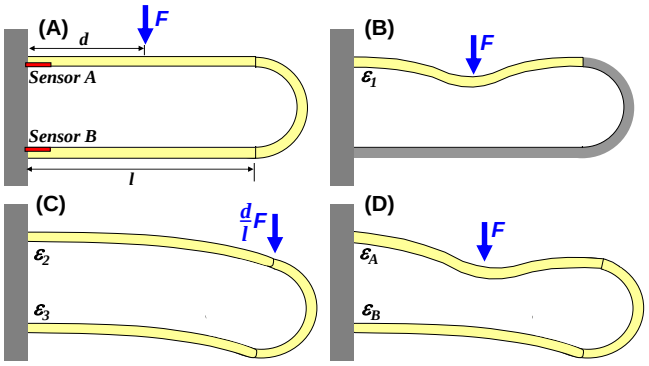

Fig. 9. 2D simplified shell structure and deformations

one point contact force is assumed in this method. Figure 11 shows a cross sectional view of the finger with four strain sensors and an applied contact force indicated. The two sensors closest to the force location will experience positive strain (positive sensor output), and the other two sensors negative strain (negative sensor output), regardless of the longitudinal location of the force, if $d > d_0$. However, since all the sensor signals must be non-negative to use the centroid method, all signal values must have the minimum signal value subtracted from them. Then, we can find the angular orientation θ of the contact force

$$\theta = \frac{\sum \phi_i S_i'}{\sum S_i'} - \alpha$$

for $i = 1, 2, 3, 4$, where $S_i' = S_i - \min\{S_1, S_2, S_3, S_4\}$, $\phi_1 = \alpha$ and $\phi_k = \phi_{k-1} + \frac{\pi}{2}$, for $k = 2, 3, 4$ (if $\phi_k \geq 2\pi$, $\phi_k = \phi_k - 2\pi$), S_i is output signal from sensor i, and α is the clockwise angle between sensor 1 and the sensor with minimum signal value.

This method produced errors less than 2°, corresponding to less than 0.5 mm on the perimeter, and an offset of 1.5° in the FEM simulation. However, experimental data gave an offset of approximately 5°, likely due to manufacturing tolerances in the placement of the sensors.

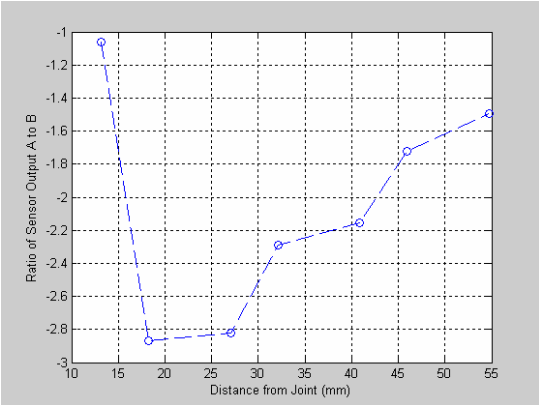

Fig. 10. Strain ratio of sensor A to B for several locations of force application along the length of the finger

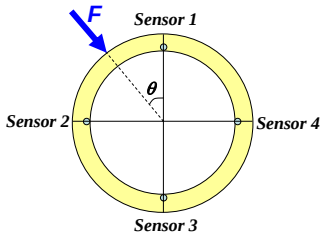

Fig. 11. Top view of the prototype showing embedded sensors and force application

VI. I-Sense™ FBG Sensor Interrogator

In the tests for this paper, the FBG sensors were interrogated by a new FBG interrogator developed by Intelligent Fiber Optic Systems Corporation (IFOS). The IFOS approach is based on a parallel photonic processing architecture which has the near-term potential to combine high channel counts (> 50 sensors on a single fiber), high resolution (submicrostrain), and high speed (> 5 kHz) with miniaturized footprint. These features will become increasingly attractive as we seek to increase the sensor number and response speed of our robotic manipulators. The ultimate goal is to have the interrogator integrated into the robotic structure as a part of monitor and control system.

As previously discussed, the application of strain on each FBG produces a shift in the wavelength that is linearly proportional to the strain. An FBG interrogator is used to precisely measure, for each FBG, the reflected wavelength shift and thus the strain applied to that FBG. Interrogators can be tunable (examining each FBG sequentially) or parallel processing in nature - The latter approach, which we use, has advantages in terms of speed particularly when dealing with many sensors.

The optical interrogator combines (a) optical signal processing (broadband light source, optical circulator, passive photonic parallel processing chip and photo-detector array) with (b) post-detection electronics, and (c) control and monitoring subsystems. Operation is as follows. The broadband source sends light through the optical circulator to an array of FBGs, each of which reflects a different Bragg wavelength. The reflected light is then returned through the optical circulator to the photonic processor which both demultiplexes the light and provides the basis for a ratiometric approach to measuring each of the returned wavelengths through conversion to different signals in various outputs from the multi-channel photodetector array. Electronics and software (or firmware) provide the final conversion of the arrayed signals to wavelength and eventually the strain to which each FBG is subjected.

Optical integration is a central technology to achieving substantial cost and size reductions for future integration. The parallel photonic processor is based on Planar Lightwave Circuit (PLC) and Arrayed Waveguide Grating (AWG) phased-array technology to separate and measure the strain-dependent wavelengths reflected by each of the multiplexed FBGs.

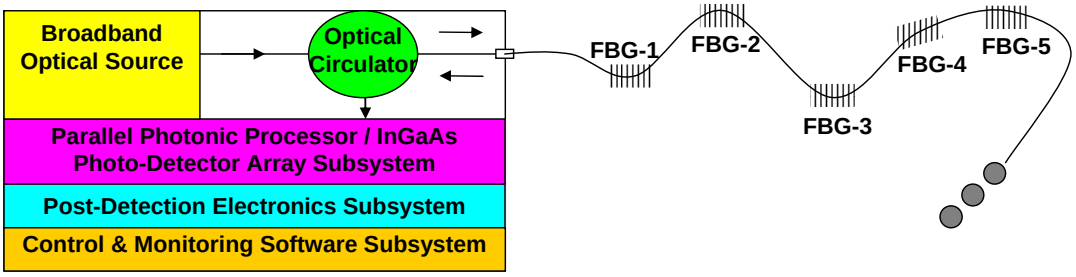

Fig. 13. Functional diagram (not-to-scale) of IFOS FBG interrogator based on a photonic parallel spectral processor which simultaneously processes signals reflected from all Fiber Bragg Gratings (FBGs).

AWGs have become increasingly popular for wavelength (de)multiplexing in WDM applications particularly for telecom and have proven to be capable of precise demultiplexing of a large number of channels with relative low losses. The basic operation principle, as shown in Figure 12, is that light propagating in the input waveguide will be coupled into the array via the first star coupler. The array has been designed such that (for the central wavelength of the demultiplexer) the optical path length difference between adjacent array arms equals an integer multiple of the central wavelength of the demultiplexer. As a consequence, the field distribution at the input aperture will be reproduced at the output aperture. Therefore, at this wavelength, the light will focus in the center of the image plane (provided that the input waveguide is centered in the input plane).

VII. Conclusions and Future Work

This article has described the development of an exoskeletal force sensing robot finger using embedded FBG optical sensors. A rapid prototyping process, shape deposition manufacturing [21] , was modified to support the fabrication of hollow, plastic mesh structures with embedded components. The fiber optic sensors were embedded near the base of a cylindrical shell with hexagonal elements for high sensitivity to imposed loads. The resulting structure is light weight and rugged. In initial experiments, the sensorized structure demonstratedmeasurement of forces of 0.01 N at frequencies of order 10 Hz. With more precise location of the sensors, higher sensitivities should be possible in the future.

and can measure forces of 0.01N at frequencies of up to 10 Hz. With more precise location of the sensors, higher sensitivities should be possible in the future.

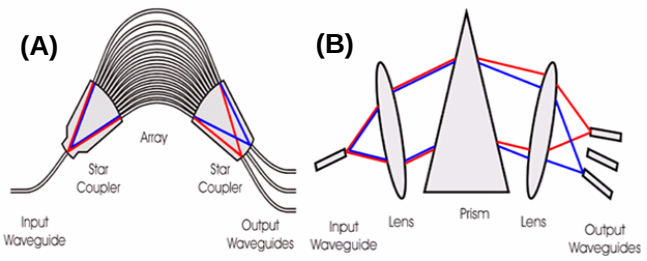

Fig. 12. Schematic representation of the phased-array demultiplexer: (A) Photonic integrated waveguid circuit, (B) Equivalent optical circuit

A copper mesh embedded in the structure reduces the amount of viscoelastic creep and provides thermal shielding. A single temperature compensation sensor at the center of the hollow finger helps to reduce the overall sensitivity to thermal variations. However the central sensor is sufficiently distant from the exterior sensors that changes in temperature do produce noticeable transient signals. This effect can be reduced in the future by using a larger number of sensors and locating thermal compensation sensors near the exterior of the structure, where they undergo the same transient thermal strains as the other sensors.

Tests were also conducted to investigate the ability to localize contact forces. Although the ability to localize forces with just four exterior sensors is limited, the results show that the mesh does respond to globally to point contacts in a predictable way. With a larger number of sensors, more accurate contact localization will be possible. Increasing the total number of sensors is relatively straightforward as multiple FBG sensors can be located along each fiber with optical multiplexing.

In parallel to the sensorized finger development, the IFOS team has been developing versions of their interrogator that support much larger sensor numbers and are smaller and considerably faster - in fact future versions are expected to support hundreds of sensors and be sensitive to acoustic and ultrasonic waves. There will remain considerable challenge in processing the data from such systems, but in the long-term such capabilities promise to take robotics far beyond its present sensor-impoverished state.

Acknowledgment

The authors thank the National Aeronautics and Space Administration (NASA) for financial support for this research through the grant from SBIR contract of NNJ06JA36C. Thanks are due to Sanjay Dastoor and Barett Heynman for their suggestions and contributions to this article.

References

[1] F. G. Barth. Spider mechanoreceptors. *Current Opinion in Neurobiology 2004*, 14:415–422, 2004.

[2] F. G. Barth and J. Stagl. The slit sense organs of arachnids. *Zoomorphologie*, 86:1–23, 1976.

[3] A. Biccihi and G. Canepa. Optimal design of multivariate sensors. *Measurement Science and Technology*, 5:319–332, 1994.

[4] A. Biccihi, J. K. Salisbury, and D. L. Brock. Contact sensing from force measurements. *International Journal of Robotics Research*, 12(3):249–262, 1993.

[5] R. Blickhan and F. G. Barth. Strains in the exoskeleton of spiders. *Journals of Comparative Physiology A*, 157:115–147, 1985.

[6] A. Dollar, C. R. Wagner, and R. D. Howe. Embedded sensors for biomimetic robotics via shape deposition manufacturing. *Proceedings of the first IEEE/RAS-EMBS International Conference on Biomedical Robotics and Biomechatronics (BioRob2006)*, 2006.

[7] W. Griffin, W. M. Provancher, and M. R. Cutkosky. Feedback strategies for telemanipulation with shared control of object handling forces. *Presence, MIT Press*, 14(6):720–731, 2005.

[8] T. C. Hales. The honeycomb conjecture. *1999, Available: http://arxiv.org/abs/math.MG/9906042*, 1999.

[9] K. O. Hill and G. Meltz. Fiber bragg grating technology fundamentals and overview. *Journal of Lightwave Technology*, 15(8), 1997.

[10] X. C. Li and F. Prinz. Metal embedded fiber bragg grating sensors in layered manufacturing. *Journal of Manufacturing Science and Engineering*, 125:577–585, 2003.

[11] S. Magne, S. Rougeault, M. Vilela, and P. Ferdinand. State-of-strain evaluation with fiber bragg grating rosettes: application to discrimination between strain and temperature effects in fiber sensors. *Applied Optics*, 36(36):9437–9447, 1997.

[12] D. T. Moran, K. M. Chapman, and R. S. Ellis. The fine structure of cockroach campaniform sensilla. *The Journal of Cell Biology*, 48:155–173, 1971.

[13] W. W. Morey, G. Meltz, and J. M.. Weiss. Recent advances in fiber bragg grating instrumentation systems. *SPIE, Self Calibrated Intelligent Optical Sensors and Systems*, SPIE-2594:90–98, 1995.

[14] I. Peterson. The honeycomb conjecture. *Science News*, 156(4):60, 1999.

[15] Y. J. Rao. In-fibre bragg grating sensors. *Measurement Science and Technology*, 8(355-375), 1997.

[16] E-A. Seyfarth, W. Eckweiler, and K. Hammer. Proprioceptors and sensory nerves in the legs of a spider, cupiennius salei (arachnida, araneida). *Zoomorphologie*, 105:190–196, 1985.

[17] D. S. Smith. The fine structure of haltere sensilla in the blowfly-calliphora erythrocephala (meig.) with scanning electron microscopic observations on the haltere surface. *Tissue and Cell*, 1:443–484, 1969.

[18] J. S. Son, M. R. Cutkosky, and R. D. Howe. Comparison of contact sensor localization abilities during manipulation. *Proceedings of 1995 IEEE/RSJ International Conference on Intelligent Robots and Systems*, 2:96–103, 1995.

[19] E. Udd. Fiber optic smart structure. *Proceedings of the IEEE*, 84(6), 1996.

[20] R. M. Voyles, G. Fedder, and P. K. Khosla. Design of a modular tactile sensor and actuatator based on an electrorheological gel. *Proceedings of the 1996 IEEE International Conference on Robotics and Automation*, 1:13–17, 1996.

[21] L. E. Weiss, R. Merz, F. B. Prinz, G. Neplotnik, P. Padmanabhan, L. Schultz, and K. Ramaswami. Shape deposition manufacturing of heterogenous structures. *Journal of Manufacturing Systems*, 16(4):239–248, 1997.

[22] M. G. Xu, J-L. Archambault, L. Reekie, and J. P. Dakin. Discrimination between strain and temperature effects using dual-wavelength fibre grating sensors. *Electronics Letters*, 30(13):1085–1087, 1994.

[23] M.G. Xu, L. Dong, L. Reekie, J.A. Tucknott, and J.L. Cruz. Temperature-independent strain sensor using a chirped bragg gratingin a tapered optical fibre. *Electronics Letters*, 31(10):823–825, 1995.